ChemPubSoc Europe

DOI: 10.1002/cctc.201300811

High Catalytic Performance of MoO_3-Bi_2SiO_5/SiO_2 for the Gas-Phase Epoxidation of Propylene by Molecular Oxygen

Yijun Pang, Xiaohui Chen,* Chengzhi Xu, Yangjun Lei, and Kemei Wei[a]

MoO_3-Bi_2SiO_5/SiO_2 catalysts with a Mo/Bi molar ratio of 5, prepared by a two-step hydrothermal and simple impregnation method, were investigated for the epoxidation of propylene by O_2 and characterized by XRD, N_2 absorption–desorption isotherms, thermogravimetric analysis (TGA), temperature-programmed reduction, NH_3 temperature-programmed desorption (TPD), and IR, Raman, and X-ray photoelectron spectroscopy (XPS). On MoO_3-Bi_2SiO_5/SiO_2 with Mo/Bi = 5 calcined at 723 K, a propylene conversion of 21.99% and a propylene oxide selectivity of 55.14% were obtained at 0.15 MPa, 673 K, and flow rates of $C_3H_6/O_2/N_2 = 1/4/20$ cm^3 min^{-1}. XRD, IR spectroscopy, and XPS results show that Bi_2SiO_5 and MoO_3 are crystalline nanoparticles. NH_3-TPD results indicate that the surface acid sites are necessary for the high catalytic activity. The results of TGA and N_2 absorption–desorption isotherms reveal that a reasonable calcination temperature is 723 K. The reaction mechanism of propylene epoxidation on MoO_3-Bi_2SiO_5/SiO_2 catalysis is hypothesized to involve an allylic radical generated at the molybdenum oxide species and the activation of O_2 at the bismuth oxide cations.

Introduction

Propylene oxide (PO) is an important chemical intermediate. In propylene derivatives, PO is the third derivative after polypropylene and acrylonitrile. At the same time, it is one of the world's top 50 of chemicals.[1] PO is applied to the production of a number of consumer goods such as polyols for the manufacture of polyurethane plastics, glycols, and monopropylene glycol and it is widely used in the chemical, pharmaceutical, food, lighting and other industries. Currently, PO is produced by two different of commercial processes: the chlorohydrin process and the hydroperoxide process.[2] However, these processes are not green chemical processes as there are a large amounts of byproducts. Therefore, there is still an urgent need to develop a new environmentally friendly process that is a one-step gas-phase reaction with O_2 as the oxidant that does not produce toxic organic waste. This route is viewed as the Holy Gail for PO production.[3]

Since a Au-Ti bimetallic catalyst was found to be an effective catalyst for gas-phase propylene epoxidation with H_2 and O_2 by Haruta's group in 1998,[4] great effort has been put into this topic.[5] The main disadvantages of this catalyst are its fast deactivation and low H_2 efficiency,[6] which means that it has a long way to go to meet industry standards[7] (propylene conversion $\geq$10%, PO selectivity $\geq$90%, H_2 efficiency $\geq$50%).

However, the Ag-catalyzed epoxidation of ethylene by O_2 has been commercialized for several decades.[2,3,8] Hu et al.[9] have reported that propylene oxidation has a similar route as ethylene epoxidation over Ag catalysts. Many types[10] of Ag catalysts have been researched but their PO selectivity is very low. The problem encountered in this heterogeneous catalysis reaction is that the PO selectivity hardly exceeds 50% if the conversion of propylene is above 10%.

However, Torres et al.[11] reported that propylene epoxidation on Ag is strongly disfavored by the markedly basic character of O_2, which leads to allylic hydrogen stripping and combustion. In contrast, the lower basicity of Cu favors metallacycle formation over PO production. A propylene conversion of 0.25% with 53% PO selectivity can be obtained over Cu/SiO_2[12] and a 1.75% PO yield can be reached over $Cu_2(OH)_3Cl/TiO_2$.[13] Wang et al.[14] have modified Cu/SiO_2 with Cs^+ to improve its catalytic performance significantly. Seubsai et al.[15] and Wang et al.[16] have studied a RuO_2-CuO-NaCl/SiO_2 catalyst that exhibits a PO selectivity of 40–50% at a propylene conversion of 10–20%.[15] In this catalyst, significant synergistic effects exist between RuO_x and CuO_x for PO formation, and direct contact between RuO_x and CuO_x may be a key factor.[16] Cu-supported catalysts can improve propylene conversion; however, the main products are combustion products and not PO.

Supported molybdenum oxide catalysts are active for a variety of reactions, such as the partial oxidation of alkanes,[17] ethers,[18] ammonia,[19] and alcohols.[20] In 2007, Song et al.[21] reported a MoO_3/SiO_2 catalyst that showed an excellent epoxidation performance. Since then, supported Mo catalysts have been seldom reported for the gas-phase epoxidation of propylene. Recently, the environmentally friendly material Bi_2SiO_5 has been reported with promising photocatalytic properties.[22] At the same time, Bi-containing materials[23] as high-performance catalysts are widely used in the epoxidation of propylene by O_2 in a one-step gas-phase reaction. Bi-Si mesoporous zeolites[24] and Bi_2SiO_5/SiO_2[25] exhibit highly selective oxidation performances. In the selective oxidation of propylene to acrolein,

[a] Y. Pang, Prof. X. Chen, Dr. C. Xu, Y. Lei, Prof. K. Wei
National Engineering Research Center for Chemical Fertilizer Catalyst
College of Chemistry and Chemical Engineering
Fuzhou University, Fuzhou, Fujian 350002 (P.R. China)
Fax:(+86) 591-83738808
E-mail: chenxhfzu@fzu.edu.cn

Bi-Mo catalysts exhibit excellent activity with 85% acrolein selectivity at a propylene conversion 50%.[26]

Although a great deal of studies have been performed on propylene epoxidation in the gas phase, there is no report of PO yields that exceed 10%.

Bimetallic catalysts, which often show electronic and chemical properties that are distinctly different from those of the parent metals, offer the opportunity to obtain new catalysts with enhanced selectivity, activity, and stability.[27] Bi-Mo oxides were widely studied for all kinds of selective oxidation during the 1960s and 1970s. Unlike previous studies that focused on Bi-Mo compounds, in this new research, Bi_2SiO_5 and MoO_3 are separate compounds that show a synergistic effect between them. In this study, MoO_3-Bi_2SiO_5/SiO_2 was prepared by a simple impregnation method and applied to the epoxidation of propylene by O_2, in which the effects of the Mo/Bi ratio, the calcination temperature, and the probable reaction mechanism were studied.

Results and Discussion

Effect of different supports

Molybdenum oxide was added to the base Bi_2SiO_5/SiO_2 catalyst, and the resulting MoO_3-Bi_2SiO_5/SiO_2 material showed an excellent catalytic performance in the epoxidation of propylene by O_2. The textural properties of the supports are shown in Table 1, and Table 2 summarizes the results of the epoxidation of propylene on molybdenum oxide supported on various materials. The conversion of propylene was 3.46% on the low-surface-area silica, whereas the conversion was 7.87% on the high-surface-area silica. With the increase of the propylene conversion, the PO selectivity increased slightly from 8.92 to 13.43% and the acrolein selectivity increased rapidly from 7.14 to 40.33%, however, the CO_x selectivity decreased from 55.04 to 33.46%.

As heterogeneous catalysis is a surface phenomenon, catalysts with a higher surface area perform better, which is often achieved by making smaller particles.[28] In addition, MoO_3 has a better dispersity on supports with high surface areas, whereas the low-surface-area supports cause bridging between the Mo species.[29] Thus, the high propylene conversion and PO selectivity may be a result of the high silica surface area, which leads to the exposure of more active sites. The MoO_3/γ-Al_2O_3 catalysts showed a very high conversion of propylene, but very low PO selectivity although γ-Al_2O_3 has a higher surface area than SiO_2-A—SiO_2-A was prepared by a method similar to the synthesis of Bi_2SiO_5/SiO_2 without the addition of Bi $(NO_3)_3$·5H_2O, whereas SiO_2-B is a commercial product. This demonstrates that the high surface area may not be the main reason for a high PO selectivity. The low PO selectivity of MoO_3/γ-Al_2O_3 can be attributed to the strong surface acidity of γ-Al_2O_3, which has a detrimental effect on PO formation and leads to combustion[30] to make CO_x the main products over MoO_3/γ-Al_2O_3. From these studies, a high surface area may not be the key factor for the high performance over MoO_3-Bi_2SiO_5/SiO_2, but significant synergistic effects between MoO_3 and Bi_2SiO_5 were discovered.

Table 1. Textural properties of the supports.

Entry	Support[a]	BET surface area [$m^2 g^{-1}$]	Pore volume [$cm^3 g^{-1}$]	Pore size [nm]
1	γ-Al_2O_3	271.8	0.51	7.6
2	SiO_2-B	139.5	0.30	8.49
3	SiO_2-A	328.4	0.86	10.48
4	Bi_2SiO_5/SiO_2	492.0	0.30	2.46

[a] γ-Al_2O_3 and SiO_2-B are commercial products. [b] SiO_2-A was prepared by a method similar to the synthesis of Bi_2SiO_5/SiO_2 without the addition of Bi $(NO_3)_3$·5H_2O.

Table 2. Catalytic performance of Mo catalysts on different supports.[a]

Support	Propylene conversion [%]	PO selectivity [%]	Acrolein selectivity [%]	CO_x selectivity [%]	Selectivity to others [%][b]
γ-Al_2O_3	16.09	0.48	7.54	85.76	6.22
SiO_2-A	3.46	8.92	7.14	55.04	28.89
SiO_2-B	7.87	13.43	40.33	33.46	12.72
Bi_2SiO_5/SiO_2	21.99	55.14	20.12	20.18	4.55

[a] All the catalysts were calcined at 723 K. Loadings of Mo: γ-Al_2O_3, SiO_2-A, and SiO_2-B were 18.3 wt% (calculated by MoO_3) and Mo/Bi = 5 (molar ratio) in Bi_2SiO_5/SiO_2. Reaction conditions: catalyst bed, 0.1 g catalyst was mixed with 2 g quartz sand; feed gas, O_2/C_3H_6/N_2 = 4:1:20 mL min^{-1}; T = 673 K; reaction pressure, 0.15 MPa. [b] Others includes carbon deposition, allyl alcohol, and other carbon-containing products, CO_x = CO_2+CO.

Effect of calcination temperature

The calcination temperature has a strong effect on the PO selectivity and the propylene conversion (Figure 1). The PO selectivity and the propylene conversion increased dramatically with the calcination temperature from 673 to 723 K. This is ascribed to the enhanced synergistic effect between MoO_3 and Bi_2SiO_5 at a higher temperature. Additionally, the catalyst particle size increased with the calcination temperature, and a moderate particle size seems to improve the catalytic performance.[31] However, if the calcination temperature was further increased, the propylene conversion decreased because of catalyst sintering, which can reduce the active centers, but the PO selectivity almost remained the same because of the presence of crystalline MoO_3,[21] which is beneficial for PO formation. The highest PO selectivity and propylene conversion were achieved over MoO_3-Bi_2SiO_5/SiO_2 calcined at 723 K.

Effect of Mo/Bi ratio

The effect of the molar ratio of Mo/Bi on the epoxidation performance of MoO_3-Bi_2SiO_5/SiO_2 is shown in Figure 2. If a small amount of molybdenum oxide was added into Bi_2SiO_5/SiO_2, for example, Mo/Bi = 1, the catalytic performance of MoO_3-Bi_2SiO_5/

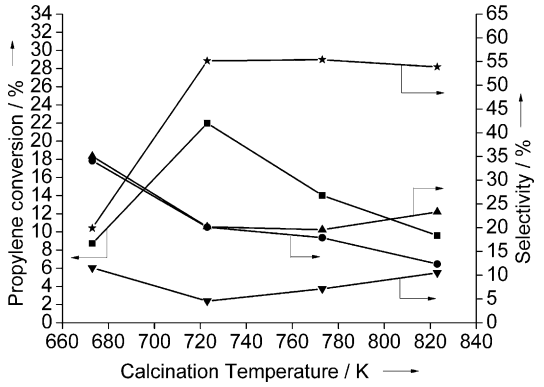

Figure 1. Catalytic activity of the MoO_3-Bi_2SiO_5/SiO_2 (Mo/Bi = 5) catalysts calcined at different temperatures. The reaction conditions are the same as those given in Table 2. Propylene conversion (■); PO selectivity (★); CO_x selectivity (▲); Acrolein selectivity (●); Selectivity to others (▼).

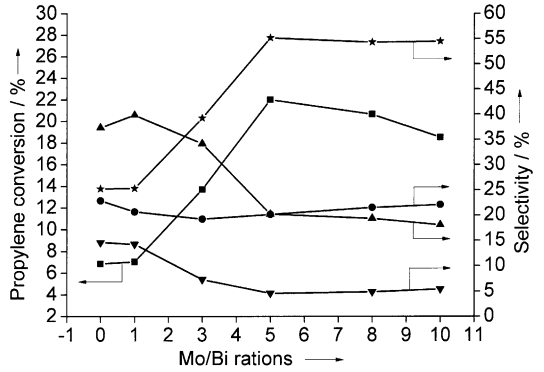

Figure 2. Effect of different Mo/Bi molar ratios on the catalytic performance of the MoO_3-Bi_2SiO_5 catalyst calcined at 723 K. The reaction conditions are the same as those given in Table 2. Propylene conversion (■); PO selectivity (★); CO_x selectivity (▲); Acrolein selectivity (●); Selectivity to others (▼).

SiO_2 was almost the same as that of Bi_2SiO_5/SiO_2 but with a higher CO_x selectivity and lower acrolein selectivity. This was because the Mo loading was too low, which led to the presence of few active sites or unmatched effects between MoO_3 and Bi_2SiO_5. However, with an increase of the Mo/Bi ratio from 1 to 5, the conversion of propylene increased sharply to a maximum and the selectivity to PO also increased. If Mo/Bi = 5, the selectivity to PO reached the maximum of 55.14% with the maximum propylene conversion of 21.99%. If the Mo/Bi ratio increased further, for example, from 5 to 10, the conversion of propylene decreased from 20.66 to 18.51% and the selectivity of PO almost remained the same. The high PO selectivity may be ascribed to the presence of crystalline MoO_3.[21] If the Mo/Bi ratio increased from 1 to 5, more active sites were formed and the MoO_3 transformed from a highly dispersed state to a crystalline state, but if the Mo/Bi ratio increased from 5 to 10, the MoO_3 agglomerated and its crystal size increased to cover the active sites, which restricts the activation of propylene. Furthermore, with an increased Mo loading, the Mo species became bridged. This increases the amount of [–O–], which disfavors C–H activation compared with [=O].[29] Therefore, the conversion of propylene decreased but the PO selectivity was almost unchanged if the Mo/Bi ratio was further increased. Additionally, the selectivity of CO_x decreased with the increase of the Mo/Bi ratio from 1 to 10. Therefore, moderate amounts of Mo oxide (Mo/Bi = 5) had the best matched effects and largely inhibited the combustion of propylene, which proves the existence of synergistic effects between the Bi_2SiO_5 and MoO_3 species.

Catalytic performance of catalysts prepared by different methods

It is assumed that crystalline MoO_3 may be favorable for the formation of PO, and the high epoxidation performance was ascribed to the synergistic effects between MoO_3 and Bi_2SiO_5. To confirm these points, catalysts prepared by different methods were investigated. No PO was detected over pure MoO_3 (Table 3), but MoO_3-Bi_2SiO_5/SiO_2 exhibited a higher epoxidation activity and a higher PO selectivity than MoO_3/SiO_2-A or MoO_3/SiO_2-B (Table 2). This further illustrates the role of crystalline MoO_3 in the catalyst.

However, if the catalytic performances of MoO_3-Bi_2SiO_5/SiO_2-A and MoO_3-Bi_2SiO_5/SiO_2-B are compared, we can see that the catalytic performance increased significantly after calcination, especially the PO selectivity. For example, after calcination, the PO selectivity increased dramatically from 20.95 to 59.91% and the propylene conversion increased from 11.62 to 15.43%. This is because MoO_3 and Bi_2SiO_5 are mixed mechanically over the MoO_3-Bi_2SiO_5/SiO_2-A catalyst and the reactive centers are not matched. After calcination, the synergistic effects were enhanced. Furthermore, the calcination temperature influences the catalyst surface acidity, which is vital for the absorption of allylic radicals in the Bi cluster cations.[32] The highest catalytic activity was obtained over MoO_3-Bi_2SiO_5/SiO_2 prepared by a simple impregnation method, which illustrates that the form of the Mo and Bi species plays a vital role in PO formation.

Table 3. Catalytic performance of Mo catalysts prepared by different methods.

Sample	Propylene conversion [%]	PO selectivity [%]	Acrolein selectivity [%]	CO_x selectivity [%]	Selectivity to others [%]
MoO_3-Bi_2SiO_5/SiO_2[a]	11.62	20.95	46.51	23.75	2.43
MoO_3-Bi_2SiO_5/SiO_2[b]	15.43	59.91	17.74	15.80	9.24
MoO_3-Bi_2SiO_5/SiO_2[c]	21.99	55.14	20.12	20.18	4.55
MoO_3[d]	2.83	0	0	12.19	87.81

Catalyst preparation: [a] MoO_3 was mechanically mixed with Bi_2SiO_5/SiO_2; [b] MoO_3 was mixed mechanically with Bi_2SiO_5/SiO_2 and then calcined at 723 K; [c] MoO_3-Bi_2SiO_5/SiO_2 was prepared as described in the Experimental Section; [d] $(NH_4)_6Mo_7O_{24}{\cdot}4H_2O$ was decomposed in air at 723 K for 8 h. The reaction conditions are the same as those given in Table 2.

Stability of MoO_3-Bi_2SiO_5/SiO_2

The stability of MoO_3-Bi_2SiO_5/SiO_2 for the epoxidation of propylene is shown in Figure 3. In the first 10 h, the PO selectivity increased from approximately 50 to 56%, and the PO selectivity remained unchanged over time. However, the conversion of propylene decreased dramatically in the first 20 h and then decreased slightly as time went by. This may be a result of the increasing particles size of MoO_3 during the propylene epoxidation reaction. The catalyst shows a good performance after 180 h (Figure 3).

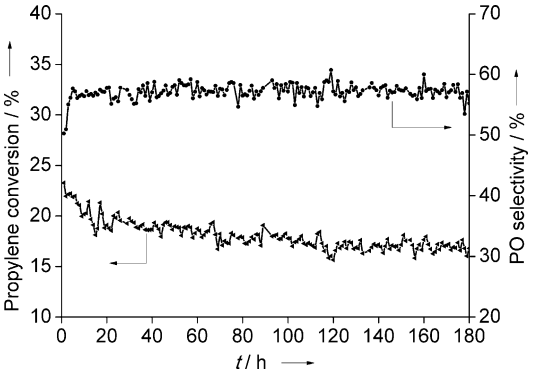

Figure 3. Time-dependent reactivity of propylene epoxidation over MoO_3-Bi_2SiO_5/SiO_2 (Mo/Bi = 5) at 673 K. The reaction conditions are the as same as those given in Table 2.

Catalyst characterization

XRD

The XRD patterns of MoO_3-Bi_2SiO_5/SiO_2 catalysts with different Mo/Bi molar ratios, calcined at different temperatures, and prepared by different methods are shown in Figures 4–6. These XRD patterns show that two crystalline species exist. The reflections at $2\theta = 21.0$, 32.6, 34.0, 36.2, and 39.4° correspond to the (012), (−221), (023), (040), and (−124) crystal faces of $Bi_2Mo_3O_{12}$ (JCPDS file: 01-078-2420), respectively. In addition, there are six strong diffraction peaks for MoO_3 (JCPDS file: 01-076-1003) at $2\theta = 14.8$, 27.1, 29.9, 31.8, 45.5, and 57.9°. The

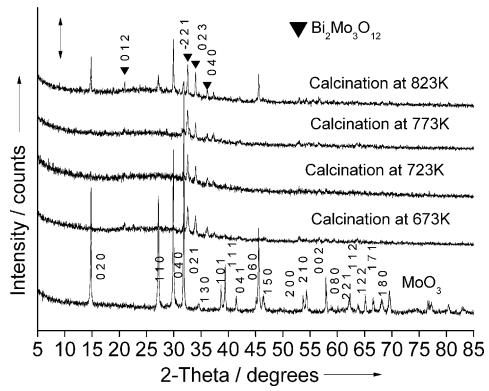

Figure 4. XRD patterns of the MoO_3-Bi_2SiO_5/SiO_2 (Mo/Bi = 5) catalysts calcined at different temperatures.

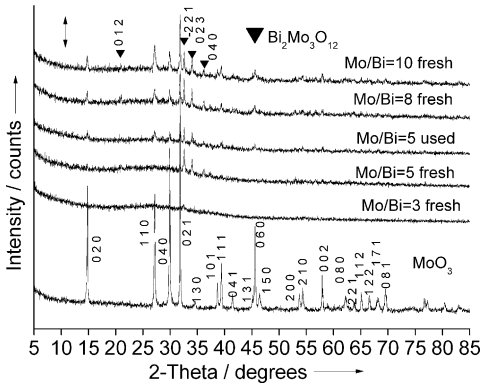

Figure 5. XRD patterns of the MoO_3-Bi_2SiO_5/SiO_2 catalysts (calcination at 723 K) with different Mo/Bi molar ratios and the used catalyst with a Mo/Bi molar ratio of 5:1.

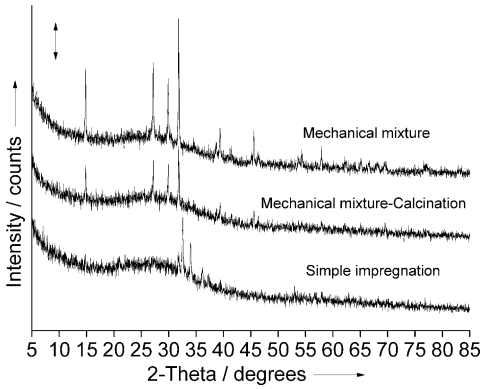

Figure 6. XRD patterns of the MoO_3-Bi_2SiO_5/SiO_2 catalysts (calcination at 723 K) prepared by different methods.

very broad band centered at $2\theta = 27.5°$ corresponds to amorphous SiO_2.

$Bi_2Mo_3O_{12}$ is present in the catalysts (Figures 4 and 5). This may be because the strong acidity of hexaammonium molybdate disrupts Bi_2SiO_5 to form $Bi_2Mo_3O_{12}$. $Bi_2Mo_3O_{12}$ oxidizes propylene to acrolein, therefore, the formation of $Bi_2Mo_3O_{12}$ is detrimental for the epoxidation of propylene. However, because the size of the MoO_3 particles are smaller than the XRD detection limit (5 nm), no crystalline MoO_3 and no Bi_2SiO_5 were detected on the catalysts by XRD if the calcination temperature was below 823 K or if the Mo/Bi ratio was below 8. After the catalyst is calcined at 823 K, the crystalline MoO_3 diffraction peaks become clearer, which also occurs if the Mo/Bi ratio increases, that is to say, the particle size of crystalline MoO_3 is increased. If the catalyst was calcined at 673, 723, and 823 K, the average particle size of $Bi_2Mo_3O_{12}$ calculated by using the Scherrer equation was 41.2, 70.1, and 181.3 nm, respectively. This demonstrates that a large particle size results from a high calcination temperature. The XRD pattern of the used catalyst is also shown in Figure 5. Compared with that of the fresh catalyst, the MoO_3 diffraction peaks are clearer. The particle size of the used catalyst was calculated by using the Scherrer equation to be 260 nm (calculations are based on the (021) crystal

face of MoO_3), but the average particle size of fresh catalyst was smaller than the XRD detection limit.

The results presented in Figure 6 show that there is no $Bi_2Mo_3O_{12}$ in the MoO_3-Bi_2SiO_5/SiO_2 catalysts prepared by mechanical blending. However, the diffraction peaks of MoO_3 are weaker after the catalyst was calcined because the average particle size decreased from 479.6 to 213.2 nm (calculations are based on the (0 2 1) crystal face of MoO_3) and the interactions between Mo species and Bi species became stronger, which reduces the crystallinity. In addition, no crystalline MoO_3 was detected on the catalysts prepared by a simple impregnation method, which demonstrated that the dispersity of Mo species is improved significantly by the impregnation method.

Thus, the good catalytic activity of MoO_3-Bi_2SiO_5/SiO_2 may be associated with nanoparticles of crystalline MoO_3. The catalyst deactivation is mainly because of the increasing particle size of MoO_3 during the propylene epoxidation reaction.

N_2 adsorption–desorption

The surface textural properties of the MoO_3-Bi_2SiO_5/SiO_2 catalysts calcined at different temperatures were measured by N_2 adsorption–desorption, and the isotherms obtained are shown in Figure 7. They are typical type IV isotherms with a hysteresis loop, representative of mesoporosity based on the IUPAC nomenclature. The hysteresis loops of the isotherms for samples A and B are H4 type, which is associated with narrow slit-like pores.[33] The hysteresis loop of the isotherm for sample C is H2 type, which is in agreement with randomly folded sheets of solids and ink-bottle-shaped pores.[33,34] The hysteresis loop of the isotherm for sample D is H3 type, which does not exhibit any limiting adsorption at high P/P^0. The H3 loop is observed with aggregates of platelike particles that give rise to slit-shaped pores.[33]

The textural properties of the catalysts are given in Table 4. Sample A calcined at 673 K had a high BET surface area. If the calcination temperature increased to 723 K, the BET surface area almost remained unchanged but the pore volume and pore size were increased. If the calcination temperature further increased, for example, from 723 to 773 K, the BET surface area dramatically decreased from 257.3 to 133.3 $m^2 g^{-1}$ and the pore size increased from 3.73 to 4.50 nm. As the temperature increased, the surface species changed from a highly dispersed state into a crystalline state. However, the catalyst was sintered if the calcination temperature increased from 773 to 823 K and the pore sizes increased dramatically from 4.50 to 14.3 nm as a result of particle accumulation.

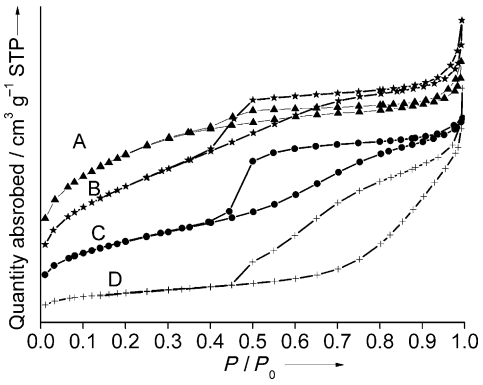

Figure 7. N_2 adsorption–desorption isotherms of MoO_3-Bi_2SiO_5/SiO_2 (Mo/Bi = 5) calcined at different temperatures. A) 673, B) 723, C) 773, and D) 823 K.

Table 4. Textural properties of MoO_3-Bi_2SiO_5/SiO_2 catalysts calcined at different temperatures.

Sample	Calcination temperature [K]	BET surface area [$m^2 g^{-1}$]	Pore volume [$cm^3 g^{-1}$]	Pore size [nm]
A	673	265.1	0.19	2.84
B	723	257.3	0.24	3.73
C	773	133.3	0.15	4.50
D	823	47.1	0.17	14.3

H_2-TPR

The temperature-programmed reduction (TPR) profiles of MoO_3-Bi_2SiO_5/SiO_2 in the range of 300–1200 K are shown in Figure 8. Over MoO_3, the main reduction peaks were between

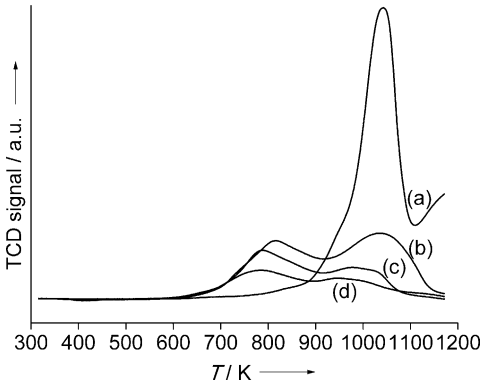

Figure 8. H_2-TPR profiles of a) pure MoO_3 and MoO_3-Bi_2SiO_5/SiO_2 b) Mo/Bi = 8, c) Mo/Bi = 5, and d) Mo/Bi = 3.

940 and 1040 K and H_2 was hardly consumed below 900 K. For the MoO_3-Bi_2SiO_5/SiO_2 samples, two main peaks were present at 650–900 and 900–1100 K assigned to the reduction of Mo^{VI} to Mo^{IV} and Mo^{IV} to Mo^0, respectively.[21] With the increased Mo loading, the intensity of the reduction peaks increased, and the peaks shifted to a higher temperature, which indicates that the Mo species were bridged, in line with the results of the catalytic activity with an increased Mo/Bi ratio.

TGA

MoO_3-Bi_2SiO_5/SiO_2 underwent weight loss on heating from 300 to 900 K (Figure 9). Nearly 50% of this loss occurred below 400 K (curves a and b). This weight loss can be attributed to the vaporization of physically adsorbed water. From 400–900 K,

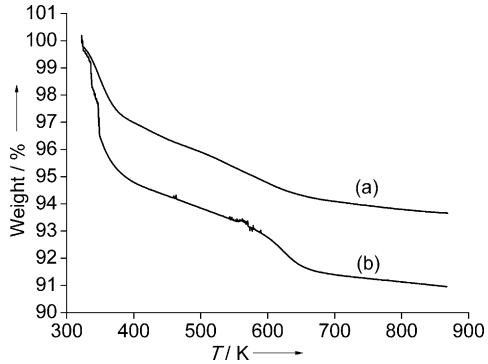

Figure 9. The weight loss curves of the a) fresh and b) used MoO_3-Bi_2SiO_5/SiO_2 catalysts (Mo/Bi = 5, calcination at 723 K).

a gradual weight loss was observed as a result of the dehydroxylation of the material. A clear weight loss was observed at 623 K, which corresponds to the intermediates from the decomposition of hexaammonium molybdate into MoO_3.[35] If we compare curves a and b, the used catalyst has a greater weight loss at 623 K, which demonstrates that under the catalytic conditions the intermediates are unstable and can prompt the transformation of intermediates to MoO_3. These results are in line with the XRD patterns of the used and fresh catalysts. Thermogravimetric analysis (TGA) indicates that calcination at 723 K is reasonable and no hexaammonium molybdate exists after calcination.

NH_3-TPD

NH_3 temperature-programmed desorption (TPD) was used to determine the acidity of the catalysts prepared at different calcination temperatures, and the results are shown in Figure 10. In the NH_3-TPD curves, the peaks are generally distributed into two regions below and above 673 K referred to as the low- (LT) and high-temperature (HT) regions, respectively. The peaks in the HT regions can be attributed to desorption of NH_3 from strong Brønsted and Lewis acid sites, and the assignment of the peaks in the LT regions is ascribed to the desorption of NH_3 from weak acid sites.[36] From the results shown in Figures 10 and 11, we can see that the calcination temperature has a significant effect on the surface acidity of the catalysts.

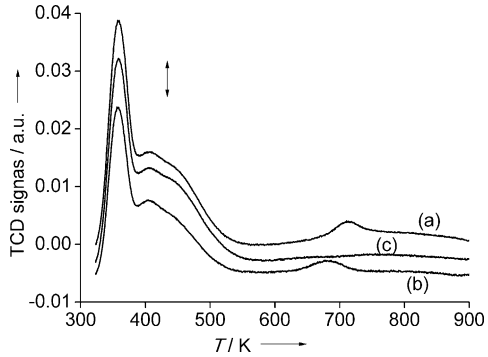

Figure 10. NH_3-TPD profiles of MoO_3-Bi_2SiO_5/SiO_2 (Mo/Bi = 5) calcined at a) 673, b) 723, and c) 773 K.

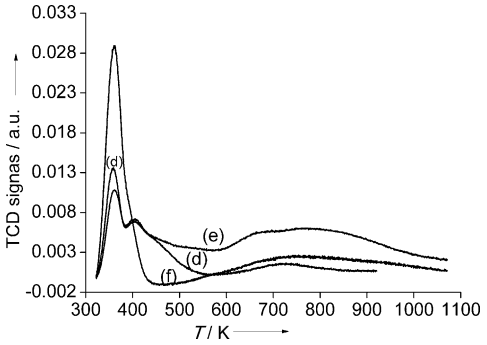

Figure 11. NH_3-TPD profiles of d) MoO_3/SiO_2, e) γ-Al_2O_3, and f) Bi_2SiO_5/SiO_2.

Peaks appeared in both the LT and HT regions of the NH_3-TPD curves of the catalysts calcined at 673 and 723 K, which confirms the existence of both weak and strong acid sites in the materials. The number of acid sites of the catalyst was reduced if the calcination temperature increased from 673 to 723 K. Additionally, the strong acid sites became weaker as the NH_3desorption temperature decreased from 710 to 673 K. Furthermore, the acid sites observed at 673 K may be vital for the high catalytic performance. If the calcination temperature was increased further, for example, to 773 K, the strong acid sites disappeared and the number of weak acid sites increased. Thus, a high calcination temperature changed the strong acid sites into weak acid sites.

The peak at 350 K is mainly ascribed to Bi_2SiO_5/SiO_5, and the peak at 410 K is mainly attributed to the Mo species (Figure 11).[10,37] A broad and weak peak of Bi_2SiO_5/SiO_2 was observed from 600–950 K, which became narrow if Mo species were introduced. Therefore, the strong acid sites on MoO_3-Bi_2SiO_5/SiO_2 are ascribed to the interactions between MoO_3 and Bi_2SiO_5, which would reduce the strong acidity of Bi_2SiO_5/SiO_2. In combination with the catalytic performance shown in Figure 1, it is easy to conclude that an appropriate amount of weak acid sites is necessary to improve the propylene conversion and strong acid sites, which led to combustion, are detrimental for the PO selectivity.

FTIR spectroscopy

The IR spectrum of Bi_2SiO_5/SiO_2 is shown in Figure 12, curve c. Five absorption bands at 462, 557, 802, 960, and 1087 cm^{-1} were observed. The band at 462 cm^{-1} is a result of the Bi–O stretching vibration.[38] The broad band at 1087 cm^{-1} accompanied by a broad shoulder centered at 1200 cm^{-1} and the weak absorption band at 557 cm^{-1} are attributed to different vibrational modes of Si–O–Si linkages.[39] The weak absorption band at 960 cm^{-1} is ascribed to the $[SiO_3]^{2-}$ tetrahedral stretching vibration, and the band at 802 cm^{-1} is a result of the Bi–O–Si stretching vibration.[38] As shown in curve a, the absorption bands at 990, 882, and 636 cm^{-1} correspond to the Mo=O stretching, Mo–O–Mo stretching, and Mo–O–Mo bending vibrations, respectively, which are typical of crystalline MoO_3 species.[37] The Bi–O–Si stretching vibration is blueshifted to 822 cm^{-1} as a result of the interaction between Bi and Mo. The

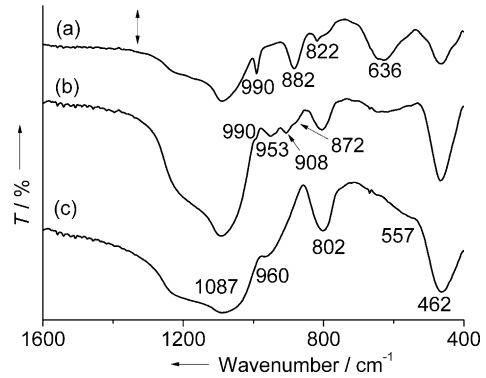

Figure 12. IR spectra of MoO_3-Bi_2SiO_5/SiO_2 prepared by a) mechanical blending and calcination and b) simple impregnation; c) IR spectrum of Bi_2SiO_5/SiO_2.

typical absorption bands of crystalline MoO_3 are also observed in the sample obtained by simple impregnation shown in Figure 12, curve b. Here, the Mo–O–Mo stretching vibration is redshifted to 872 cm^{-1}, and the Mo=O stretching and Mo–O–Mo bending vibrations are weaker, which is ascribed to the stronger interactions between MoO_3 and Bi_2SiO_5/SiO_2. The two weak absorption bands at 908 and 953 cm^{-1} can be attributed to surface Si=OH and the formation of an Mo=O=Si bond from the interaction between the Mo species and the silica surface.[40] Moreover, two bands can be attributed to the Mo–O vibrations of bismuth molybdate. The IR studies demonstrate that crystalline MoO_3 and Bi_2SiO_5 exist in MoO_3-Bi_2SiO_5/SiO_2 if Mo/Bi = 5. The IR studies are in line with the XRD patterns (Figure 5) and the catalytic performance given in Table 4.

Raman spectroscopy

The Raman spectra of the MoO_3-Bi_2SiO_5/SiO_2 catalysts calcined at different temperatures are displayed in Figure 13. Bulk MoO_3 is evidenced by the bands at 995, 820, and 666 cm^{-1} and the doublet at 286 and 291 cm^{-1} if the catalyst was calcined at 723 K.[41] The band at 995 cm^{-1} is assigned to the symmetric stretching mode of the terminal Mo=O groups, the doublet bands at 286 and 291 cm^{-1} are attributed to the two wagging modes of the terminal Mo=O groups, and the signals at 820 and 666 cm^{-1} are assigned to the vibrations of the Mo–O–Mo bridge in crystalline MoO_3.[42] Notably, no bulk MoO_3 is seen if the catalysts are calcined at a higher temperature of 773 K or a lower temperature of 673 K. The bands at low frequency (not labeled) may be attributed to Bi_2SiO_5.

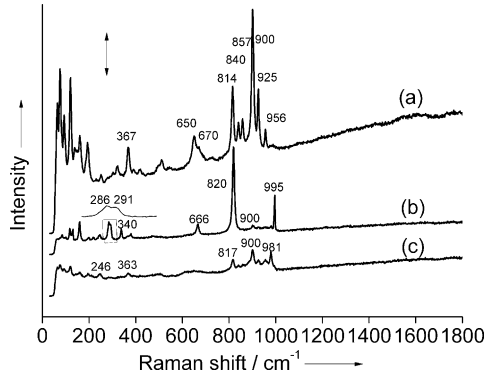

Figure 13. Raman spectra of MoO_3-Bi_2SiO_5/SiO_2 catalysts calcined at a) 773, b) 723, and c) 673 K.

XPS

The X-ray photoelectron spectra (XPS) of MoO_3-Bi_2SiO_5/SiO_2 are presented in Figures 14 and 15. As shown in Figure 14, the binding energy (BE) of Mo $3d_{5/2}$ and Mo $3d_{3/2}$ is 232.60 and 235.80 eV, respectively. This is very similar to the standard BE of MoO_3 (232.65 and 235.85 eV), which shows that the Mo species are Mo^{6+} and exist as the main form of MoO_3. The Bi 4f XPS spectra are shown in Figure 15, and the BE of Bi $4f_{7/2}$ and Bi $4f_{5/2}$ is 159.39 and 164.78 eV, respectively, which shows that the Bi species are Bi^{3+}. Combined with the IR spectra shown in Figure 12, this shows that Bi exists mainly as Bi_2SiO_5. For the MoO_3-Bi_2SiO_5/SiO_2, the BE of Mo $3d_{5/2}$ and Bi $4f_{7/2}$ is 232.60 and 159.39 eV, respectively. Compared with the BE of Mo $3d_{5/2}$ of MoO_3 (232.65 eV) and Bi $4f_{7/2}$ of Bi^{3+} compounds (159.30 eV), the Bi species is electron deficient (evidenced by the BE increase of Bi $4f_{7/2}$), and Mo^{6+} probably obtains the electrons from Bi species (evidenced by the BE decrease of Mo $3d_{5/2}$), which may be associated with the interaction between the Mo and Bi species.

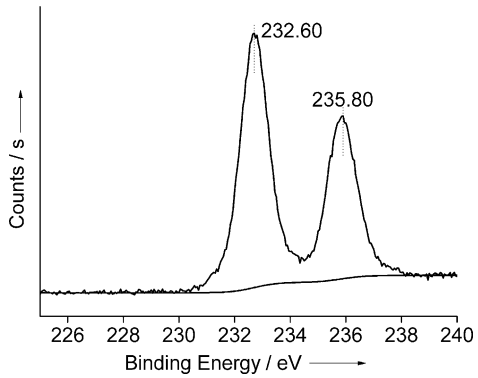

Figure 14. XPS Mo 3d spectrum of MoO_3-Bi_2SiO_5/SiO_2.

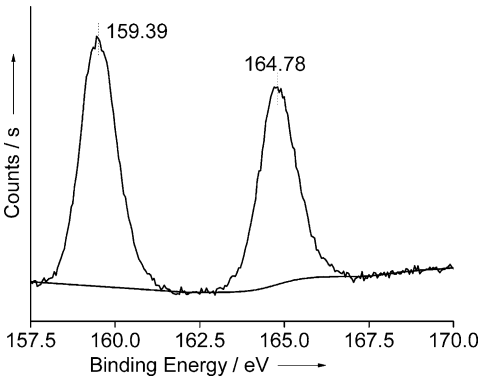

Figure 15. XPS Bi 4f spectrum of MoO_3-Bi_2SiO_5/SiO_2.

Probable synergistic effects between MoO_3 and Bi_2SiO_5 in the propylene epoxidation reaction

Bi_2SiO_5 in an orthorhombic system that exhibits a 2D structure[43] in space built from the intergrowth of $(SiO_3)^{2-}$ layers with the insertion of $(Bi_2O_2)^{2+}$ layers. The $(Bi_2O_2)^{2+}$ layers are formed from a distorted square oxygen plane with alternately capping Bi atoms above and below this square oxygen plane. Oxidation processes that involve heterogeneous catalysts usually occur through the adsorption and activation of O_2. A probable mechanism is shown in Scheme 1.

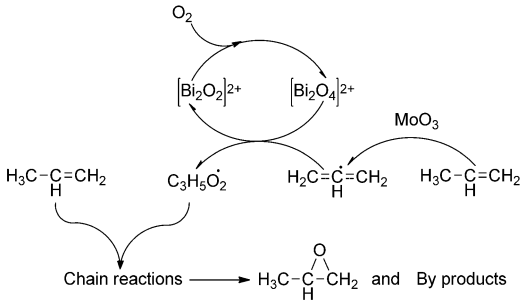

Scheme 1. Proposed synergistic effect between MoO_3 and Bi_2SiO_5 in propylene epoxidation.

In previous studies,[23c,31] bismuth oxide cluster cations have been shown to play an important role in the presence of O_2 for the oxidation of alkenes, and bismuth oxide cluster cations are a possible reactive center for the activation of O_2.[23c] Similarly, the $(Bi_2O_2)^{2+}$ layers may also be a possible reactive center for the activation of O_2, which would form an intermediate $(Bi_2O_4)^{2+}$.

At the same time, molybdenum oxides with a terminal [=O] group may serve as the reactive center for the activation of C–H bonds.[29] It may be easy to abstract allylic hydrogen atoms to form allylic radicals.[21,30] Then, the allylic radicals can be absorbed on $(Bi_2O_4)^{2+}$[23c] and desorption occurs to form a superoxide allylic radical species.[23b] The superoxide allylic radical then reacts in a chain reaction[44] to form PO. The surface acidity has a significant effect on the catalytic activity (Figure 10), which is ascribed to the acid sites that play an important role in the absorption of allylic radicals on $(Bi_2O_4)^{2+}$. Furthermore, the reactions that occur in the Bi species are kinetically favorable,[32] so they may be fast. However, the activation of propylene and the abstraction of H that occurred on the Mo species may not be as easy as the activation of O_2. Therefore, the formation of allylic radicals may be the rate-determining step. These assumptions are in line with the Mo/Bi ratio shown in Figure 2.

Conclusion

A MoO_3-Bi_2SiO_5/SiO_2 catalyst, which was prepared in a two-step hydrothermal and simple impregnation method, exhibits good performance and stability in the epoxidation of propylene. The most favorable synergistic effects between Bi and Mo species are found with a Mo/Bi molar ratio of 5:1. The reactive centers consist of nanoparticulate crystalline MoO_3 that activates the propylene and bismuth oxide cluster cations that activate O_2. The appropriate calcination temperature is 723 K after which the catalyst has a considerable specific surface area and moderate amounts of surface acid, both of which have considerable influence on the catalytic activity.

Experimental Section

Preparation of catalysts

The synthesis of Bi_2SiO_5/SiO_2 (Si/Bi = 50)

Bi_2SiO_5/SiO_2 was prepared using the method reported previously.[25] Typically, hexadecyl trimethyl ammonium bromide (0.25 g; CTAB, Sinopharm Chemical Reagent Co., Ltd, AR) was dissolved in deionized water (30 mL) with automatic stirring for 1 h in an ice-water bath. Then of tetraethyl orthosilicate (5.2 g; TEOS, Sinopharm Chemical Reagent Co., Ltd, AR) was added dropwise into above solution, and the homogeneous mixture was labeled as solution A. At the same time, $Bi(NO_3)_3{\cdot}5H_2O$ (0.24 g; Sinopharm Chemical Reagent Co., Ltd, AR) was dissolved in aqueous glycerol solution (5 mL, 50 vol%) and labeled as solution B. Solution A was allowed to stand for 1 h, then solution B was added dropwise into solution A with a constant stirring speed, and a white suspension solution was obtained. After 1 h, the mixture was transferred into a Teflon-lined autoclave with a capacity of 50 mL, and the autoclave was sealed and heated under autogenous pressure at 353 K for 20 h. The sample was cooled to RT and the solid product was collected and washed with deionized water three times with filtration. The obtained white solid precipitate was dried at 383 K for 12 h and calcined at 823 K for 8 h in air to give Bi_2SiO_5/SiO_2.

Mo loading process

The supported Mo catalysts were prepared by a simple impregnation method. Bi_2SiO_5/SiO_2 powder ($\approx$1.6 g) was added to deionized water (30 mL) with stirring for $\approx$30 min in an ice-water bath. Then a quantity of hexaammonium molybdate ($(NH_4)_6Mo_7O_{24}{\cdot}4H_2O$, Shanghai Colloid Chemical Plant, AR) was added into the suspension solution, which was kept in the ice-water bath with stirring. After 10 h, the mixture was dried at 383 K overnight and calcined at different temperatures for 8 h in air to give MoO_3-Bi_2SiO_5/SiO_2. The preparation of the other catalysts was similar, and the different supports and their properties are shown in Table 1.

Catalytic reaction

The catalytic reactions were performed in a stainless-steel downflow reactor with an inner quartz tube under a pressure of 0.15 MPa at 673 K with a flow rate of 25 mL min^{-1}. The catalyst (0.1 g) was mixed with quartz sand (2.0 g, 24–50 mesh) and placed in the central zone of the reactor. Propylene mixed with O_2 and N_2 carrier gas were delivered by mass-flow controllers at flow rates of $C_3H_6/O_2/N_2 = 1/4/20$ mL min^{-1}. The reaction pressure was kept at 0.15 MPa, and the reactor was then heated. The reaction products were analyzed by on-line GC equipped with a thermal conductivity detector (TCD), GDX-403-packed column, and a six-way valve manual injector. The column temperature was controlled by a temperature program. The initial column temperature was 323 K,

which was held for 1.5 min, and then the column temperature was increased to 383 K at a rate of 15 K min^{-1}, which was held for 10 min. All the other lines and valves between the exit of the reactor and the chromatograph were heated to 403 K to prevent the condensation of the products.

Catalyst characterization

The XRD patterns of the samples were obtained by using a diffractometer operated at 40 kV and 40 mA with CoK_α radiation ($\lambda =$ 1.62083 nm) over a 2θ range between 5–85° and scanned at the speed of 0.2088° s^{-1} with a step size of 0.0167°. The surface areas and pore diameter distributions were measured by N_2 absorption–desorption at 77 K by using a volumetric unit (Micromeritics ASAP 2020). Prior to the adsorption measurements, the samples were pretreated for 1 h in a N_2 steam at 523 K. TPR and NH_3-TPD were performed by using an Autochem II 2920 instrument equipped with a TCD detector. For H_2-TPR, the samples (≈50 mg) were pretreated at 573 K in a He flow (30 mL min^{-1}) for 30 min, cooled to 303 K, and swept with a He flow. The reducing gas was a mixture of 10 vol% H_2/Ar (30 mL min^{-1}), and the temperature was increased at 10 K min^{-1} from 303 to 1173 K. For NH_3-TPD, the samples (≈0.1 g) were pretreated in Ar at 573 K for 1 h before the was NH_3 adsorbed. The NH_3-TPD experiments were performed from 323–923 K in a flow of Ar (30 mL min^{-1}). The heating rate was 10 K min^{-1}. TGA was performed by using a Perkin–Elmer TGA7 instrument. The samples (3–5 mg) were treated at 323 K in an air flow (20 mL min^{-1}) for 5 min before the temperature was increased at 10 K min^{-1} from 323–873 K. FTIR spectra were recorded by using a Nicolet 6700 FTIR spectrometer (4000–400 cm^{-1}), and the sample was ground with KBr and pressed into thin wafer. Raman spectra were measured at RT by using an instrument with a microscope attachment (inVia Reflex, Renishaw Company, UK) by using 532 nm as the excitation radiation. XPS spectra were recorded by using a Thermo ESCALAB 250 spectrometer with a monochromatized AlK_α X-ray source, and a passing energy of 30 eV. The C 1s (BE = 284.6 eV) of adventitious carbon was used as the reference.

Acknowledgements

Support by the National Natural Science Foundation of China (Grant Nos.20976030) and the New Century Excellent Talents in Fujian province (HX2006-100) is acknowledged.

Keywords: bismuth · epoxidation · molybdenum · oxygen · polymers

[1] M. Eissen, J. O. Metzger, E. Schmidt, U. Schneidewind, *Angew. Chem.* **2002**, *114*, 402–425; *Angew. Chem. Int. Ed.* **2002**, *41*, 414–436.
[2] T. A. Nijhuis, M. Makkee, J. A. Moulijn, B. M. Weckhuysen, *Ind. Eng. Chem. Res.* **2006**, *45*, 3447–3459.
[3] M. McCoy, *Chem. Eng. News* **2001**, *79*, 19–20.
[4] T. Hayashi, K. Tanaka, M. Haruta, *J. Catal.* **1998**, *178*, 566–575.
[5] a) G. Zhan, M. Du, J. Huang, Q. Li, *Catal. Commun.* **2011**, *12*, 830–833; b) B. S. Uphade, M. Okumura, S. Tsubota, M. Haruta, *Appl. Catal. A* **2000**, *190*, 43–50.
[6] B. Chowdhury, J. J. Bravo-Suárez, N. Mimura, J. Lu, K. K. Bando, S. Tsubota, M. Haruta, *J. Phys. Chem. B* **2006**, *110*, 22995–22999.
[7] A. K. Sinha, S. Seelan, S. Tsubota, M. Haruta, *Angew. Chem.* **2004**, *116*, 1572–1574; *Angew. Chem. Int. Ed.* **2004**, *43*, 1546–1548.
[8] J. R. Monnier, *Appl. Catal. A* **2001**, *221*, 73–91.
[9] Z.-M. Hu, H. Nakai, H. Nakatsuji, *Surf. Sci.* **1998**, *401*, 371–391.
[10] a) G. Jin, G. Lu, Y. Guo, Y. Guo, J. Wang, W. Kong, X. Liu, *J. Mol. Catal. A* **2005**, *232*, 165–172; b) J. Lu, J. J. Bravo-Suárez, M. Haruta, S. T. Oyama, *Appl. Catal. A* **2006**, *302*, 283–295; c) W. Yao, Y. L. Guo, X. H. Liu, Y. Guo, Y. Q. Wang, Y. S. Wang, Z. G. Zhang, G. Z. Lu, *Catal. Lett.* **2007**, *119*, 185–190; d) G. Lu, X. Zuo, *Catal. Lett.* **1999**, *58*, 67–70.
[11] D. Torres, N. Lopez, F. Illas, R. M. Lambert, *Angew. Chem.* **2007**, *119*, 2101–2104.
[12] O. P. Vaughan, G. Kyriakou, N. Macleod, M. Tikhov, R. M. Lambert, *J. Catal.* **2005**, *236*, 401–404.
[13] J. Qiang-wei, W. Kai-xue, W. Jian-qiang, L. Xiao-bei, C. Jie-sheng, *Chem. Res. Chin. Univ.* **2011**, *27*, 866–869.
[14] J. He, Q. Zhai, Q. Zhang, W. Deng, Y. Wang, *J. Catal.* **2013**, *299*, 53–66.
[15] A. Seubsai, M. Kahn, S. Senkan, *ChemCatChem* **2011**, *3*, 174–179.
[16] W. Long, Q. Zhai, J. He, Q. Zhang, W. Deng, Y. Wang, *ChemPlusChem* **2012**, *77*, 27–30.
[17] K. Chen, A. T. Bell, E. Iglesia, *J. Catal.* **2002**, *209*, 35–42.
[18] H. Liu, E. Iglesia, *J. Catal.* **2002**, *208*, 1–5.
[19] a) J. D. Burrington, R. K. Grasselli, *J. Catal.* **1979**, *59*, 79–99; b) J. D. Burrington, C. T. Kartisek, R. K. Grasselli, *J. Catal.* **1980**, *63*, 235–254.
[20] M. Brandhorst, S. Cristol, M. Capron, C. Dujardin, H. Vezin, E. Payen, *Catal. Today* **2006**, *113*, 34–39.
[21] Z. Song, N. Mimura, J. J. Bravo-Suárez, T. Akita, S. Tsubota, S. T. Oyama, *Appl. Catal. A* **2007**, *316*, 142–151.
[22] a) X. Feng, X. Qi, J. Li, L. Yang, M. Qiu, J. Yin, F. Lu, J. Zhong, *Appl. Surf. Sci.* **2011**, *257*, 5571–5575; b) L. Zhang, W. Wang, S. Sun, J. Xu, M. Shang, J. Ren, *Appl. Catal. B* **2010**, *100*, 97–101; c) R. Chen, J. Bi, L. Wu, W. Wang, Z. Li, X. Fu, *Inorg. Chem.* **2009**, *48*, 9072–9076.
[23] a) Z. Zhao, T. Kobayashi, *Appl. Catal. A* **2001**, *207*, 139–149; b) D. Barreca, F. Morazzoni, G. A. Rizzi, R. Scotti, E. Tondello, *Phys. Chem. Chem. Phys.* **2001**, *3*, 1743–1749; c) A. Fielicke, K. Rademann, *J. Phys. Chem. A* **2000**, *104*, 6979–6982.
[24] X. Chen, J. Su, K. Wei, *J. Chem. Ind. Eng.* **2004**, *55*, 1815–1820.
[25] Y. Zhong, X. Chen, K. Wei, *Ind. Catal.* **2012**, *20*, 1–5.
[26] J. Peacock, A. Parker, P. Ashmore, J. Hockey, *J. Catal.* **1969**, *15*, 398–406.
[27] J. G. Chen, C. A. Menning, M. B. Zellner, *Surf. Sci. Rep.* **2008**, *63*, 201–254.
[28] N. R. Shiju, *ChemCatChem* **2011**, *3*, 112–114.
[29] G. Fu, X. Xu, X. Lu, H. Wan, *J. Am. Chem. Soc.* **2005**, *127*, 3989–3996.
[30] B. Horváth, M. Hronec, *Appl. Catal. A* **2008**, *347*, 72–80.
[31] B. Horváth, M. Hronec, I. Vávra, M. Šustek, Z. Križanová, J. Dérer, E. Dobročka, *Catal. Commun.* **2013**, *34*, 16–21.
[32] M. Bienati, V. Bonačic-Koutecký, P. Fantucci, *J. Phys. Chem. A* **2000**, *104*, 6983–6992.
[33] R. Pierotti, J. Rouquerol, *Pure Appl. Chem.* **1985**, *57*, 603–619.
[34] J. Sánchez-Valente, X. Bokhimi, F. Hernandez, *Langmuir* **2003**, *19*, 3583–3588.
[35] A. Said, *Thermochim. Acta* **1994**, *236*, 93–104.
[36] a) M. Sawa, M. Niwa, Y. Murakami, *Zeolites* **1990**, *10*, 532–538; b) F. Lónyi, J. Valyon, *Microporous Mesoporous Mater.* **2001**, *47*, 293–301.
[37] Y. Miao, G. Lu, X. Liu, Y. Guo, Y. Wang, Y. Guo, *J. Ind. Eng. Chem.* **2010**, *16*, 45–50.
[38] X.-J. Dai, Y.-S. Luo, S.-Y. Fu, W.-Q. Chen, Y. Lu, *Solid State Sci.* **2010**, *12*, 637–642.
[39] E. R. Lippincott, A. Van Valkenburg, C. E. Weir, E. Bunting, *J. Res. Natl. Bur. Stand.* **1958**, *61*, 61–70.
[40] A. Said, A. El-Aziz, M. M. Abd El-Wahab, *J. Chem. Technol. Biotechnol.* **2006**, *81*, 329–335.
[41] S. Braun, L. G. Appel, V. L. Camorim, M. Schmal, *J. Phys. Chem. B* **2000**, *104*, 6584–6590.
[42] G. Mestl, T. Srinivasan, *Catal. Rev.* **1998**, *40*, 451–570.
[43] S. Georges, F. Goutenoire, P. Lacorre, *J. Solid State Chem.* **2006**, *179*, 4020–4028.
[44] a) J. B. Reitz, E. I. Solomon, *J. Am. Chem. Soc.* **1998**, *120*, 11467–11478; b) D. J. Driscoll, K. D. Campbell, J. H. Lunsford, *Adv. Catal.* **1987**, *35*, 139–186; c) H. Orzesek, R. P. Schulz, U. Dingerdissen, W. F. Maier, *Chem. Eng. Technol.* **1999**, *22*, 691–700.

Received: September 24, 2013
Revised: November 21, 2013
Published online on February 5, 2014